The Astrophysical Journal, 655:940–945, 2007 February 1

ULTRAVIOLET EXCITED HIGH-J MOLECULAR HYDROGEN IN PHOTODISSOCIATION REGIONS

Dae-Hee Lee,[1] Soojong Pak,[2] W. Van Dyke Dixon,[3] and Ewine F. van Dishoeck[4]

Received 2006 May 17; accepted 2006 October 18

ABSTRACT

We have calculated synthetic interstellar cloud models to investigate the formation and destruction of high-J molecular hydrogen in photodissociation regions. The effects of five physical parameters (the incident ultraviolet [UV] intensity, H_2 column density, cloud temperature, total density, and H_2 formation rate coefficient) on the populations of H_2 rotational levels are explored. We have found that $N(4)/N(0)$ is proportional to the incident UV intensity I_{UV} and the H_2 molecular fraction f is simply related to the ratio of I_{UV} and the hydrogen density n_H, implying a new method to derive I_{UV} and n_H with the observational parameters $N(4)/N(0)$ and f, assuming an H_2 formation rate R. High-resolution *FUSE* spectra of H_2 toward three translucent sight lines (HD 110432, HD 192639, and HD 185418) in the Milky Way and 24 diffuse sight lines in the SMC and LMC are referenced to obtain $N(4)/N(0)$ and f. Using our method, we are able to derive $I_{UV} \sim 10-40$ for the translucent sight lines, when R is assumed to be 10 times higher than the Galactic value. Synthetic models for the Magellanic sight lines suggest that $I_{UV} \geq 10$, $n_H \leq 100$ cm^{-3}, and $R \sim 3 \times 10^{-16}$ for the low H_2 column density sight lines ($N[H_2] \leq 10^{18}$ cm^{-2}) and $I_{UV} \geq 10$, $n_H \leq 1000$ cm^{-3}, and $R \sim 3 \times 10^{-17}$ for the high H_2 column density sight lines ($N[H_2] \geq 10^{19}$ cm^{-2}).

Subject headings: ISM: clouds — line: profiles — ultraviolet: ISM

Online material: color figures

1. INTRODUCTION

The hydrogen molecule (H_2) is the most abundant molecule in the interstellar medium (ISM). Numerous systematic measurements of H_2 absorption in the far-ultraviolet (FUV), e.g., the *Copernicus* satellite (Savage et al. 1977), the Hopkins Ultraviolet Telescope (Blair et al. 1996), *ORFEUS* (Richter 2000; Dixon et al. 1998), and the *Far Ultraviolet Spectroscopic Explorer* (*FUSE*; Shull et al. 2000; Snow et al. 2000), have derived the values of $N(J)$, the column density of H_2 in the rotational level J of the ground vibrational and electronic state, and compared them with theoretical predictions to study H_2 formation, destruction, and excitation in the ISM.

Many theoretical efforts have explored the steady state relationships between the physical parameters and $N(J)$ through the cloud (Jura 1975a, 1975b; Black & Dalgarno 1976, 1977; van Dishoeck & Black 1986, hereafter VDB86; Black & van Dishoeck 1987, hereafter BVD87; Sternberg 1989). For example, one may infer the kinetic temperature of the clouds from $N(1)/N(0)$ (Shull & Beckwith 1982), while Jura (1975a, 1975b) has shown that one can calculate Rn, the product of formation rate and density, and estimate the incident UV flux from a comparison between detailed numerical calculations and the observations of $N(4)/N(0)$ and $N(5)/N(1)$, which are controlled by the optical pumping rate (see Lee et al. [2000, 2002] for a comparison). Indeed, the ratios $N(4)/N(0)$ and $N(5)/N(1)$ serve as measures of the UV radiation field, while $N(2)/N(0)$ and $N(3)/N(1)$ determine the collision rate (Shull & Beckwith 1982). Browning et al. (2003) have used detailed H_2 models to obtain constraints on otherwise unobservable parameters of the Large and Small Magellanic Clouds (LMC and SMC, respectively) by reproducing the observed $N(J)$ terms. Determination of the physical parameters of the LMC and SMC is important, e.g., for interpretation of the diffuse interstellar band (DIB) spectra in terms of the physicochemical properties of the different DIB carriers (Ehrenfreund et al. 2002; Cox et al. 2006).

Recently, Gry et al. (2002) and Falgarone et al. (2005) argued the existence of warm gas in the cold diffuse ISM based on the *FUSE* and *ISO* Short Wavelength Spectrometer (SWS) observations, respectively, suggesting that H_2 molecules in $J \geq 3$ levels are excited mainly by collisions in warm regions. However, most of their excited H_2 column density $N(H_2^*)$ is in $J = 3$ at the temperature of <1000 K inferred for this warm gas; significant population of the higher levels $J \geq 4$ would require temperatures >1000 K. The lack of a well-established physical model to compute the amount and temperature of warm gas due to dissipation of magnetohydrodynamic (MHD) turbulence prevents a more quantitative assessment and a direct comparison with UV pumping. In this study we therefore focus only on UV photon pumping for the high-J H_2 populations in gas that is too cold for significant collisional excitation.

We present the results of plane-parallel photodissociation region (PDR) H_2 model calculations to investigate the high-J H_2 populations following UV excitation and compare the models with the cited observational results. Although there have been a number of efforts to model molecular hydrogen in various interstellar clouds, our study is distinct from the earlier work, because it presents the first systematic study of the high-J H_2 populations for a wide range of model parameters and compares the model results with new observational data from *FUSE* for a large sample of clouds, including the low-metallicity SMC and LMC sight lines. We also suggest a new method for deriving I_{UV} and n_H with the observational parameters $N(4)/N(0)$, $N(H_2)$, and f, using our models. We have chosen $N(4)/N(0)$, although $N(4)$ is rather uncertain, as it lies on the flat part of the curve of growth, because there are more observational data of $N(4)$ than $N(5)$. In § 2 we describe the H_2 model and introduce the input parameters for the

[1] Korea Astronomy and Space Science Institute, Daejoen, South Korea; dhlee@kasi.re.kr.
[2] Department of Astronomy and Space Science, Kyung Hee University, Gyeonggi-do, South Korea; soojong@khu.ac.kr.
[3] Department of Physics and Astronomy, The Johns Hopkins University, Baltimore, MD; wvd@pha.jhu.edu.
[4] Sterrewacht Leiden, RA Leiden, The Netherlands; ewine@strw.leidenuniv.nl.

models. In § 3 we plot model results and describe our interpretation. In § 4 we compare the models with high-resolution *FUSE* data. Finally, we summarize our conclusions in § 5.

2. MODEL CALCULATIONS

We have used the PDR H_2 model developed by VDB86 and BVD87. The model program considers the abundance and excitation of H_2 in plane-parallel clouds, includes all 211 bound levels of all vibrational levels, $v = 0$–14, of the $X\,^1\Sigma_g^+$ state of H_2 with J up to an arbitrary limit of 15, and treats explicitly the rates of all electronic transitions into the $B\,^1\Sigma_g^+$ and $C\,^1\Pi_u$ states involving these levels. Photoionization out of excited H_2 levels with $v \geq 4$ is included explicitly, and the effects of direct photodissociation out of $v \geq 3$ are considered. It is assumed that the abundance of H_2 is governed in steady state primarily by the rate of formation on grain surfaces and the rates of destruction by spontaneous fluorescent dissociation following absorption in the $B\,^1\Sigma_g^+$–$X\,^1\Sigma_g^+$ Lyman and $C\,^1\Pi_u$–$X\,^1\Sigma_g^+$ Werner band systems. The model assumptions are valid provided the density is less than 10^5 cm^{-3} and temperature less than 1000 K, when collisional excitation and de-excitation of vibrationally excited levels start to become important (VDB86, BVD87). Since the H_2 UV excitation is very rapid (<1000 yr for a standard diffuse cloud) the assumption of steady state is also justified. The equation of transfer is solved for 22,445 absorption lines simultaneously with the equations of statistical equilibrium that describe the populations of 211 levels of $X\,^1\Sigma_g^+$ ($v = 0$–14, $J \leq 15$), 629 levels of $B\,^1\Sigma_g^+$ ($v = 0$–36, $J \leq 16$), and 476 levels of $C\,^1\Pi_u$ ($v = 0$–13, $J \leq 16$). Our calculations involve multiple pumping, i.e., excitation of $H_2(v \geq 1)$, which starts to become important when the ultraviolet radiation field is 10^3 or more times as intense as the mean interstellar radiation field (Shull 1978, BVD87). The program calculates the dissociation and excitation rates, densities, and column densities of all vibrational and rotational levels of H_2 through the model cloud, including H_2 self-shielding and continuum shielding by dust.

The model requires several input parameters, such as the total hydrogen density $n_{\rm H}$, the cloud temperature T, the total H_2 column density $N(H_2)$, the spectrum and intensity of the incident UV radiation field $I_{\rm UV}$, and the H_2 formation rate coefficient, y_f, which is related to the formation rate R, in its simplest form, as

$$R = 3 \times 10^{-18} T^{1/2} y_f. \quad (1)$$

The term $I_{\rm UV}$ is the enhancement factor compared with the mean interstellar value adopted by Draine (1978), i.e., $\phi(\lambda = 1000\ \text{Å}) = 4.5 \times 10^{-8}$ photons cm^{-2} s^{-1} Hz^{-1} when $I_{\rm UV} = 1$. For the standard values of $y_f = 1$ and $T = 100$ K, the derived H_2 formation rates are consistent with the more elaborate results from Cazaux & Tielens (2002). We have calculated models for each of 1080 combinations of these five parameters: $n_{\rm H} = 10$, 10^2, 10^3 cm^{-3}; $T = 10$, 100, 200 K; $N(H_2) = 10^{14}$, 10^{15}, 10^{16}, 10^{17}, 10^{18}, 10^{19}, 10^{20}, 10^{21} cm^{-2}; $I_{\rm UV} = 10^{-1}$, 10^0, 10^1, 10^2, 10^3; and $y_f = 0.1$, 1, 10. In more realistic diffuse cloud models, the gas temperature and total density will vary with position. However, in the relatively narrow part of the cloud where most of the UV pumping occurs, the temperature and total density can be taken to be constant. For example, VDB86 presented diffuse cloud models with varying temperature and density with depth for which the results do not differ significantly from those with constant physical parameters. In addition, the cloud depth of the H/H_2 transition region, where most of the H_2 is excited, is less than 10^{16} cm (see Fig. 1 in BVD87), so the effects of gradients are negligible.

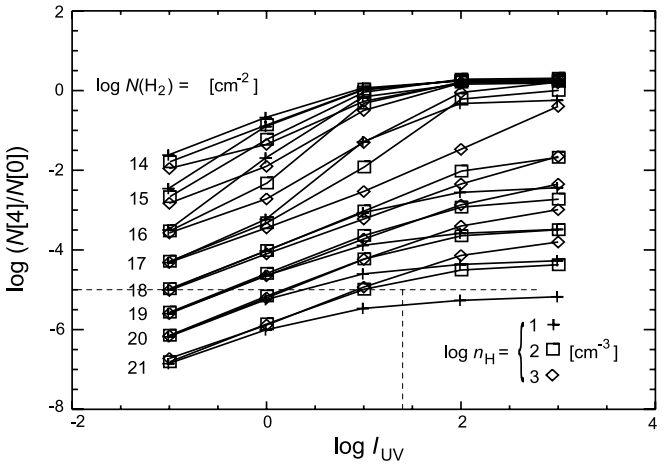

FIG. 1.—Model calculations results of $\log[N(4)/N(0)]$ vs. $I_{\rm UV}$ with 24 combinations of eight values of $N(H_2)$ and three values of $n_{\rm H}$. Other parameters are set as $T = 100$ K and $y_f = 10$. Three $n_{\rm H}$ values are distinguished by shapes: $\log n_{\rm H} = 1$ cm^{-3} (*plus signs*), $\log n_{\rm H} = 2$ cm^{-3} (*squares*), and $\log n_{\rm H} = 3$ cm^{-3} (*diamonds*). Dashed lines stand for the line of sight toward HD 192639, discussed in § 4.1. [*See the electronic edition of the Journal for a color version of this figure.*]

We adopt the standard interstellar values described in BVD87 for the remaining parameters, which have relatively less influence on high-J levels; e.g., we have used the dust model from Roberge et al. (1991), which has a moderately large albedo $\omega \sim 0.5$ and is partly forward scattering, with $g \sim 0.5$ at the relevant wavelength $\lambda = 912$–1200 Å. Wagenblast (1992) argued that the H_2 formation mechanism, not UV pumping, could be important. The BVD87 models consider three possible distributions following the formation of H_2 on grains: (1) one-third of the 4.5 eV binding energy is deposited statistically as internal excitation, (2) the entire population is in $v = 14$, with statistical distribution over $J = 0$ and 1, and (3) the entire population is in $v = 6$, J with the rotational population characterized by the grain temperature. We have tested these H_2 formation models and that from Wagenblast (1992) to see the effects of the initial population of H_2 on formation. The formation model from Wagenblast assumes that all populations are in $v = 5$, with a statistical distribution over $J = 9$ and 10. The test results show that only Wagenblast's model has some effects on the high-J populations, especially for low H_2 column densities ($N[H_2] \leq 10^{16}$ cm^{-2}), compared to the others that produce similar results to each other. Since the number of such cases is small even in the Wagenblast model, we have used formation model (3), in which newly formed molecules appear with an amount of vibrational excitation comparable in energy to the difference between the binding energy of the molecule and the depth of a potential well on an amorphous silicate surface (i.e., $v < 7$) for our analysis.

3. RESULTS AND ANALYSIS

3.1. $N(4)/N(0)$ *versus Incident UV Intensity*

The dependence of $N(4)/N(0)$ on $I_{\rm UV}$ is explored in Figure 1, where $N(4)/N(0)$ is plotted versus $I_{\rm UV}$ with 24 combinations of eight $N(H_2)$ values and three $n_{\rm H}$ values, while T and y_f are fixed (see Fig. 1 caption for details). There are three things to note in Figure 1. First, when $N(H_2)$ is high, $N(4)/N(0)$ is low, independent of the other parameters. This is reasonable, because the fraction of the outer shell of a cloud that is excited by a given incident UV flux becomes smaller if the cloud becomes thicker. In other words, the fraction of cloud where self-shielding prevents the excitation of H_2 is larger when $N(H_2)$ is higher. Second,

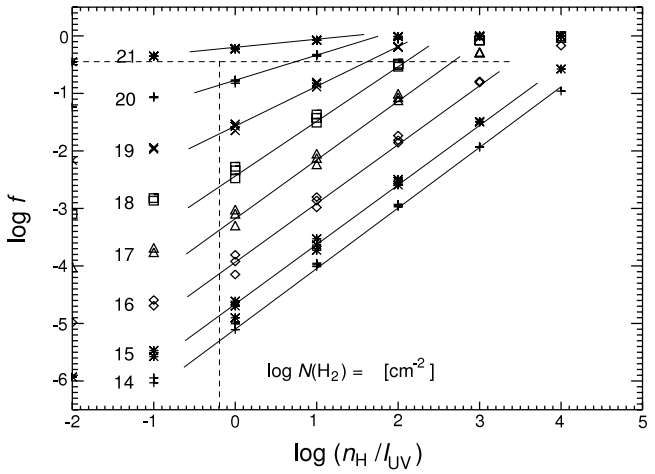

FIG. 2.—Model calculation results of $\log f$ vs. $\log (n_H/I_{UV})$ for eight values of $N(H_2)$ using $T = 100$ K, $y_f = 10$, and $n_H = 10$–1000 cm^{-3}. Dashed lines are the observed values for the line of sight toward HD 192639. Each symbol represents the $\log[N(H_2)]$ column density ranging from 14 to 21.

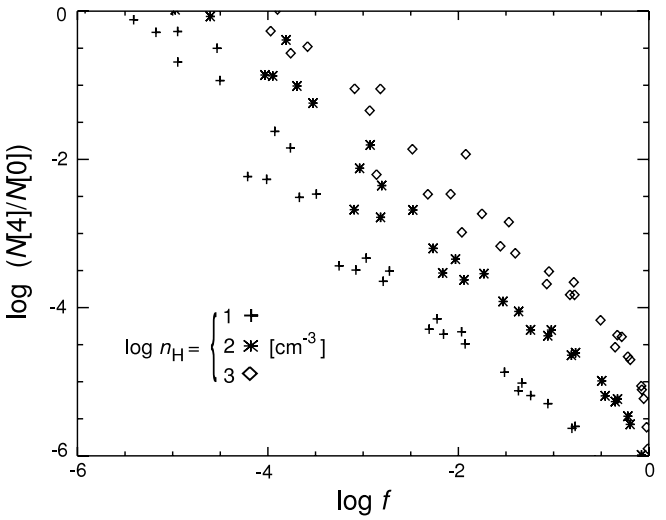

FIG. 3.—Model calculation results of $\log[N(4)/N(0)]$ vs. $\log f$ for three values of n_H using $T = 100$ K, $y_f = 1$, $I_{UV} = 0.1$–1000, and $\log N(H_2) = 14$–21 cm^{-2}.

for a given $N(H_2)$, $N(4)/N(0)$ is proportional to I_{UV}, consistent with the findings by Lee et al. (2000), although it eventually saturates as I_{UV} becomes higher. This limit to the $N(4)/N(0)$ ratio mainly results from the lack of self-shielding of the H_2 molecules because there is so much photodissociation at high I_{UV}. Finally, when I_{UV} is low, the $N(4)/N(0)$ values in each group are close to each other, regardless of n_H, while the $N(4)/N(0)$ values diverge for higher values of I_{UV} and $N(H_2)$. In all cases, the optical depths at 1000 Å by the H_2 self-shielding and the dust absorption are comparable when the ratio I_{UV}/n_H is of order unity (BVD87). When $I_{UV}/n_H \ll 1$, line absorption completely dominates the attenuation of the UV radiation, and most of the available photons dissociate and excite H_2, which produces the same $N(4)/N(0)$ ratio, independent of n_H. When $I_{UV}/n_H \gg 1$, the absorption of UV photons by grains becomes important; if the cloud is thick enough, then some of the photons are removed by the grains, so the efficiency of H_2 excitation is reduced. This means that the presence of an intense UV radiation field will not yield the maximum $N(4)/N(0)$ ratio unless the density n_H is also large, which is easily seen in Figure 1.

3.2. *Molecular Fraction versus Incident UV Intensity and Hydrogen Density*

Not all observed quantities serve as reliable indicators of physical parameters such as density, temperature, and UV radiation field. On the other hand, some model parameters must be assumed, because they cannot be observed directly. From this perspective, the H_2 molecular fraction f is useful for comparing the models with observational results, because f is easily obtained from observations,

$$f = \frac{2N(H_2)}{N(H\ I) + 2N(H_2)}. \quad (2)$$

In determining f observationally, a bias can be induced, because part of the atomic H may arise in diffuse atomic clouds along the line of sight, unrelated to the targets. This is considered in § 4.

Assuming a steady state in the boundary layer of a cloud where $n(H_2) \ll n(H) \sim n_H$,

$$\log f \propto -\log I_{UV} + \log n_H + \tfrac{1}{2}\log T + \log y_f, \quad (3)$$

or

$$\log f \propto \log(n_H/I_{UV}), \quad (4)$$

from equation (14) in BVD87.

With this in mind, we present the models with a moderately high H_2 formation rate, $n_H = 10$–1000 cm^{-3}, $T = 100$ K, and $y_f = 10$, i.e., $R = 3 \times 10^{-16}$, to plot $\log f$ versus $\log (n_H/I_{UV})$ with eight values of $N(H_2)$ in Figure 2. The reason we have chosen such models in Figure 2 is explained in § 4.1. The same plot with a typical interstellar value $y_f = 1$ is almost identical to Figure 2, except $\log f$ is about 0.5–1 dex lower overall. Figure 2 clearly shows that $\log f$ scales linearly with $\log (n_H/I_{UV})$ when $\log (n_H/I_{UV}) > 0$, regardless of the hydrogen density. Note that equation (4) is not appropriate at high $N(H_2)$, where $n(H) \not\sim n_H$, but the linear relation between $\log f$ and $\log (n_H/I_{UV})$ still holds. In the case of $\log (n_H/I_{UV}) < 0$, I_{UV}/n_H becomes greater than 1, absorption of the incident UV photons by grains becomes important so that the dissociation of H_2 is reduced.

We combine the results of Figures 1 and 2 to remove the dependence on I_{UV} in Figure 3, which shows three features: (1) $\log[N(4)/N(0)]$ is inversely proportional to $\log f$, (2) the slope is determined by $N(H_2)$, and (3) the y-intercept is determined by n_H. Feature (1) is plausible in the sense that both $\log[N(4)/N(0)]$ and $\log f$ are affected by $\log I_{UV}$; the former positively, while the latter negatively. Feature (2) can be understood as a result of the self-shielding; $\log f$ is changing more rapidly along with $\log I_{UV}$ when $N(H_2)$ is smaller, because self-shielding makes the absorption of UV photons followed by dissociation of hydrogen molecules slow when $N(H_2)$ becomes larger. The y-intercept of the plot $\log[N(4)/N(0)]$ versus $\log f$ indicates the value of $\log[N(4)/N(0)]$ at the maximum point of the H_2 formation (or H_2 dissociation in steady state) with given parameters n_H, y_f, and $T^{1/2}$ (see eq. [3]). If we assume a value of the H_2 formation rate R in the target cloud, then the effect of y_f and T is not significant. So, n_H mainly determines the y-intercept value of $\log[N(4)/N(0)]$, feature (3). These features imply that we can obtain n_H directly from the observational parameters $N(H_2)$, $N(4)/N(0)$, and f and, consequently, I_{UV} from Figure 1. Practical applications of this result follow in § 4.

4. DISCUSSION

4.1. *The Translucent Clouds*

We have applied our models to high-resolution *FUSE* spectra of three sight lines toward HD 110432 (Rachford et al.

TABLE 1
PHYSICAL PARAMETERS OF THREE TRANSLUCENT SIGHT LINES

Sight Lines	n_H (cm^{-3})	T (K)	$N(H_2)$ (cm^{-2})	log f	log $[N(4)/N(0)]$	log $(n_H/I_{UV})^4$	log $I_{UV}{}^4$	log $n_H{}^4$
HD 110432[1]	~200	63 ± 7	20.68 ± 0.05	−0.24 ± 0.09	−4.27 ± 0.45	0.6	1.6	2.2
HD 192639[2]	16 ± 3	90 ± 10	20.76 ± 0.21	−0.44 ± 0.11	−5.00 ± 0.25	−0.2	1.4	1.2
HD 185418[3]	6.3 ± 2.5	100 ± 15	20.71 ± 0.21	−0.36 ± 0.11	−5.30 ± 0.30	0	1.0	1.0

[1] From Rachford et al. (2001).
[2] From Sonnentrucker et al. (2002).
[3] From Sonnentrucker et al. (2003).
[4] Derived in this study.

2001), HD 192639 (Sonnentrucker et al. 2002), and HD 185418 (Sonnentrucker et al. 2003). Table 1 shows the observed parameters of these sight lines with error ranges (a detailed description of the error analysis is given in the above papers) and the derived parameters I_{UV} and n_H from our models. The way these values have been obtained as follows; find the corresponding log (n_H/I_{UV}) to observed log f and $N(H_2)$ in Figure 2. Then, one can determine n_H and I_{UV} in Figure 1 by applying $\log[N(4)/N(0)]$ and the derived n_H/I_{UV} value. This means that one can easily estimate n_H and I_{UV} from the observational parameters without actual model calculations. The example for the sight line toward HD 192639 is indicated in Figures 1 and 2 as dashed lines. Strictly speaking, the product Rn_H rather than n_H is obtained from the data. However, because n_H has been inferred independently for these lines of sight from other observations, R can be determined.

The resulting UV intensities of the three translucent sight lines are 10–40 times the interstellar average value, which are rather high, given the fact that these clouds are not necessarily close to the background bright OB stars. It should be noted that our best-fit models imply an H_2 formation rate $y_f = 10$. Rachford et al. (2001) and Sonnentrucker et al. (2003) reported high-J H_2 column densities that could not be explained by an average interstellar radiation field. Part of the problem may be solved by adopting a higher formation rate in the sight lines. Our best-fit models, $T =$ 100 K and $y_f = 10$, imply R to be 3×10^{-16}, which is about 10 times the average interstellar value. Habart et al. (2004) and Li et al. (2002) reported such a high H_2 formation rate in regions of moderate incident FUV intensity ($I_{UV} \sim 100$) based on the *ISO* results and discussed the cause of the higher formation rate. In conclusion, our analysis indicates that the H_2 observations are only

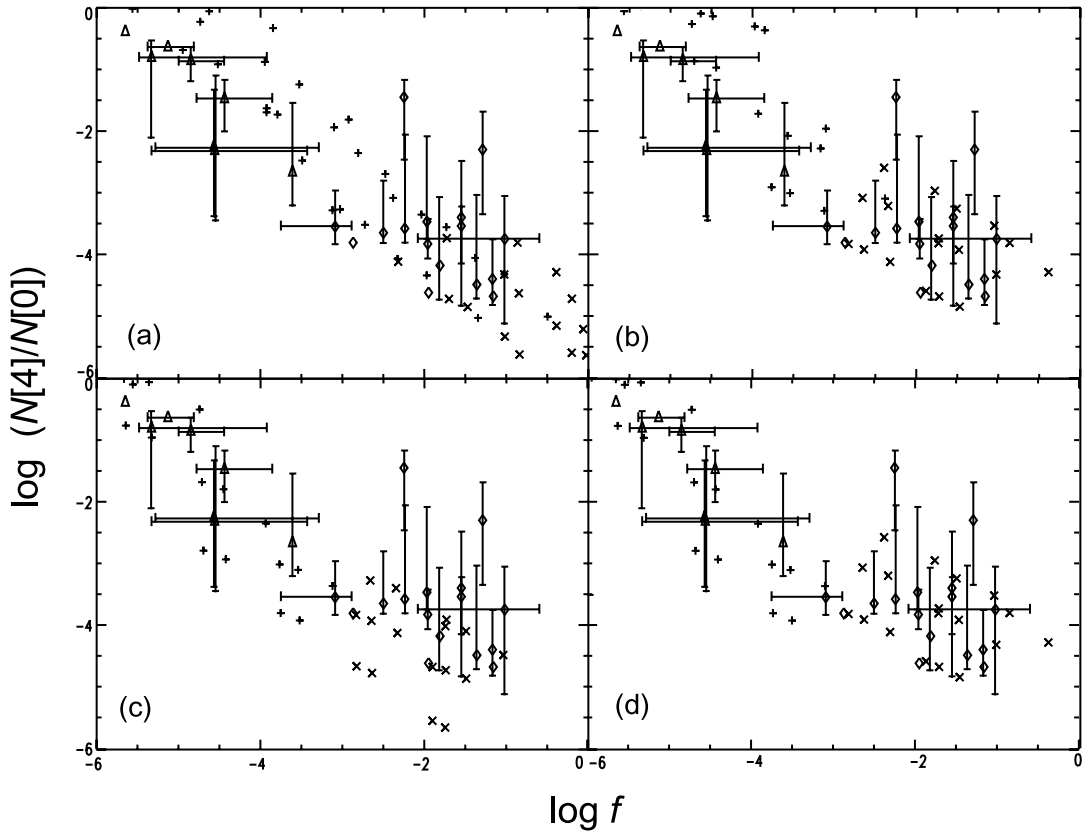

FIG. 4.—Comparison of observed (*triangles and diamonds*) and simulated (*crosses and plus signs*) relations between $\log[N(4)/N(0)]$ and $\log f$. The Magellanic sight lines with lower ($\leq 10^{18}$ cm^{-2}) and higher ($\geq 10^{19}$ cm^{-2}) column densities are plotted as triangles and diamonds, respectively. When the uncertainty of a value is greater than 0.1 dex, its error bar is plotted. Model results are overplotted as follows: (*a*) $I_{UV} = 0.1$–10 and $y_f = 1$, (*b*) $I_{UV} = 10$–1000 and $y_f = 1$, (*c*) $I_{UV} = 10$–1000 and $y_f = 0.1$, and (*d*) $I_{UV} = 10$–1000 and $y_f = 0.1$ when $N(H_2) \leq 10^{18}$ cm^{-2} and $y_f = 1$ when $N(H_2) \geq 10^{19}$ cm^{-2}. Other parameters set are $T = 100$ K and $n_H = 10$–100 cm^{-3} when $N(H_2) \leq 10^{18}$ cm^{-2} and $n_H = 10$–1000 cm^{-3} when $N(H_2) \geq 10^{19}$ cm^{-2}. [*See the electronic edition of the Journal for a color version of this figure.*]

consistent with previously inferred densities if an enhanced H_2 formation rate is assumed.

4.2. *The Small and Large Magellanic Clouds*

Tumlinson et al. (2002) surveyed 70 sight lines to the SLC and LMC with *FUSE*. Of these, 47 sources exhibit absorption lines from the H_2 Lyman and Werner bands. We have used the 24 targets for which Tumlinson et al. report $N(4)$ column densities. The $N(4)/N(0)$ versus f for the 24 targets is shown in Figure 4 as triangles when $N(H_2) \leq 10^{18}$ cm^{-2} and as diamonds when $N(H_2) > 10^{18}$ cm^{-2}. Error bars, taken from Tumlinson et al., are plotted only when they are greater than 0.1 dex. The plotted values of f include the correction for systematic errors in the Galactic N(H I) column described in § 2.4 of Tumlinson et al. (2002).

We have reproduced the observational results with our models. Because of the low metallicity of the SMC/LMC, we have set the gas-to-dust ratio of the Magellanic Clouds as 4 times higher than that of the Galactic clouds in our models (Pak et al. 1998). The lower dust abundance affects both the amount of dust extinction as well as the grain surface area available for H_2 formation. To verify this, we have made four model grids: Figure 4*a* $I_{UV} = 0.1$–10 and $y_f = 1$, Figure 4*b* $I_{UV} = 10$–1000 and $y_f = 1$, Figure 4*c* $I_{UV} = 10$–1000 and $y_f = 0.1$, and Figure 4*d* $I_{UV} = 10$–1000 and $y_f = 0.1$ when $N(H_2) \leq 10^{18}$ cm^{-2} and $y_f = 1$ when $N(H_2) \geq 10^{19}$ cm^{-2}. Other parameters set are $T = 100$ K and $n_H = 10$–100 cm^{-3} when $N(H_2) \leq 10^{18}$ cm^{-2} and $n_H = 10$–1000 cm^{-3} when $N(H_2) \geq 10^{19}$ cm^{-2}. Low column density models are plotted in Figure 4 as plus signs, while high column density models are plotted as crosses. Figure 4*d* shows that the model grid, which has high incident UV intensity and a low H_2 formation rate coefficient at low H_2 column density sight lines but a Galactic H_2 formation rate coefficient at high H_2 column density sight lines, reproduces the observed results well. An intermediate value of y_f, say $y_f = 0.3$, for both high and low column density sight lines might reproduce the observed results of SMC and LMC as well. However, Richter (2000) suggested based on *ORFEUS* data that the H_2 formation rate may be higher in clouds with a higher molecular fraction region. Accordingly, we have treated the high and low column density sight lines differently. Tumlinson et al. (2002) argued that the models with a lower H_2 formation rate reproduced the Magellanic sight lines well in their Figure 9*d*. However, that is the case for only the sight lines with $\log f < -3$. One can see that the models with $y_f = 1$ reproduce the Magellanic sight lines well with $\log f > -3$ in their Figure 9*c*. Since our models also support this conclusion in Figure 4, we have used $y_f = 1$ for modeling Magellanic sight lines of high H_2 column densities.

From these results, we draw the following conclusions. (1) For low column density clouds ($N[H_2] \leq 10^{18}$ cm^{-2}), the hydrogen densities are around 10–100 cm^{-3}, the incident UV intensities are 10 times or more higher than the interstellar value and the formation rate coefficient is as low as 0.1, which is consistent with the argument that the H_2 formation rate in the SMC and LMC is 3–10 times lower than the Galactic mean value (Tumlinson et al. 2002). (2) For high column density clouds ($N[H_2] > 10^{18}$ cm^{-2}), hydrogen densities range from 10 to more than 1000 cm^{-3}, $I_{UV} \geq 10$, and y_f is 1, closer to the interstellar value. It should be noted that the individual observed points in Figure 3 can be reproduced by many other models that have different combinations of input parameters. However, only our interpretation results in a reasonable range of physical parameters for the collective observational data of the Magellanic Clouds.

5. CONCLUSION

A plane-parallel PDR H_2 model developed by BVD87 is used to investigate the UV-excited high-J H_2 populations in interstellar clouds. In this model, assuming a steady state between H_2 formation and destruction in a cloud, a total of 1080 synthetic model calculations with five independent physical parameters successfully produce the linear relation between $N(4)/N(0)$ and I_{UV}. We also find that the molecular fraction $\log f$ is inversely proportional to the logarithm of incident UV intensity I_{UV} divided by the hydrogen density n_H. Therefore, we are able to set the value of both I_{UV} and n_H from the observational parameters $N(4)/N(0)$, $N(H_2)$, and f, if we assume the molecular formation rate R.

Three translucent sight lines and 24 diffuse sight lines in the SMC and LMC observed by *FUSE* are introduced for comparison with our models. In the case of the translucent sight lines, we present a simple way to derive the incident UV intensity as well as the hydrogen density using our model plots. The resulting UV intensities range from 10 to 40 times the interstellar value. Since these translucent sight lines have hydrogen densities inferred from other data, we can use the H_2 observations to obtain an H_2 formation rate 10 times higher than the interstellar value.

For the Magellanic sight lines, we select model grids with $n_H \sim 10$–100 cm^{-3}, $I_{UV} \geq 10$, and $y_f = 0.1$ for the low column density clouds ($N[H_2] \leq 10^{18}$ cm^{-2}), and $n_H \sim 10$–1000 cm^{-3}, $I_{UV} \geq 10$, and $y_f = 1$ for the high column density clouds ($N[H_2] > 10^{18}$ cm^{-2}) to reproduce the observed results, which means a different H_2 formation rate between the low and high H_2 column density regions in the Magellanic Clouds. A second set of diffuse molecular clouds, surveyed by *ORFEUS*, will be investigated in the same manner in the near future.

The authors are grateful to Bastiaan Jonkheid for assistance with the models. S. P. was financially supported by grant R01-2005-000-10610-0 from the Basic Research Program of the Korea Science and Engineering Foundation.

REFERENCES

Black, J. H., & Dalgarno, A. 1976, ApJ, 203, 132
———. 1977, ApJS, 34, 405
Black, J. H., & van Dishoeck, E. F. 1987, ApJ, 322, 412 (BVD87)
Blair, W. P., Long, K. S., & Raymond, J. C. 1996, ApJ, 468, 871
Browning, M. K., Tumlinson, J., & Shull, J. M. 2003, ApJ, 582, 810
Cazaux, S., & Tielens, A. G. G. M. 2002, ApJ, 575, L29
Cox, N. L. J., Cordiner, M. A., Cami, J., Foing, B. H., Sarre, P. J., Kaper, L., & Ehrenfreund, P. 2006, A&A, 447, 991
Dixon, W. V., Hurwitz, M., & Bowyer, S. 1998, ApJ, 492, 569
Draine, B. T. 1978, ApJS, 36, 595
Ehrenfreund, P., et al. 2002, ApJ, 576, L117
Falgarone, E., Verstraete, L., Pineau des Forêts, G., & Hily-Blant, P. 2005, A&A, 433, 997
Gry, C., Boulanger, F., Nehme, C., Pineau des Forêts, G., Habart, E., & Falgarone, E. 2002, A&A, 391, 675
Habart, E., Boulanger, F., Verstraete, L., Walmsley, C. M., & Pineau des Forêts, G. 2004, A&A, 414, 531
Jura, M. 1975a, ApJ, 197, 575
———. 1975b, ApJ, 197, 581
Lee, D.-H., Min, K. W., Dixon, W. V., Hurwitz, M., Ryu, K. S., Seon, K. I., & Edelstein, J. 2000, ApJ, 545, 885
Lee, D.-H., et al. 2002, ApJ, 575, 234

Li, W., Evans, N. J., II, Jaffe, D. T., van Dishoeck, E. F., & Thi, W.-F. 2002, ApJ, 568, 242
Pak, S., Jaffe, D. T., van Dishoeck, E. F., Johansson, L. E. B., & Booth, R. S. 1998, ApJ, 498, 735
Rachford, B. L., et al. 2001, ApJ, 555, 839
Richter, P. 2000, A&A, 359, 1111
Roberge, W. G., Jones, D., Lepp, S., & Dalgarno, A. 1991, ApJS, 77, 287
Savage, B. D., Bohlin, R. C., Drake, J. F., & Budich, W. 1977, ApJ, 216, 291
Shull, J. M. 1978, ApJ, 219, 877
Shull, J. M., & Beckwith, S. 1982, ARA&A, 20, 163
Shull, J. M., et al. 2000, ApJ, 538, L73
Snow, T. P., et al. 2000, ApJ, 538, L65
Sonnentrucker, P., Friedman, S. D., Welty, D. E., York, D. G., & Snow, T. P. 2002, ApJ, 576, 241
———. 2003, ApJ, 596, 350
Sternberg, A. 1989, ApJ, 347, 863
Tumlinson, J., et al. 2002, ApJ, 566, 857
van Dishoeck, E. F., & Black, J. H. 1986, ApJS, 62, 109 (VDB86)
Wagenblast, R. 1992, MNRAS, 259, 155